NASA
Technical Memorandum 81443

AVRADCOM
Technical Report TR-80-C-7

COMPOSITE WALL CONCEPT FOR HIGH TEMPERATURE TURBINE SHROUDS - SURVEY OF LOW MODULUS STRAIN ISOLATOR MATERIALS

Robert C. Bill
Propulsion Laboratory
AVRADCOM Research and Technology Laboratories

and

Gordon P. Allen and Donald W. Wisander
Lewis Research Center
Cleveland, Ohio

Prepared for the
Twenty-Fifth Annual International Gas Turbine Conference
sponsored by the American Society of Mechanical Engineers
New Orleans, Louisiana, March 9-13, 1980

COMPOSITE WALL CONCEPT FOR HIGH TEMPERATURE TURBINE SHROUDS - SURVEY OF LOW MODULUS STRAIN ISOLATOR MATERIALS

by

Robert C. Bill
Propulsion Laboratory

Lewis Research Center

and

Gordon P. Allen and Donald W. Wisander
Lewis Research Center
Cleveland, Ohio 44135

E-363

ABSTRACT

Plasma-sprayed yttria stabilized zirconium oxide turbine seal specimens, incorporating various low modulus porous metal strain isolator pads between the zirconium oxide and a dense metal substrate, were subjected to cyclic thermal shock testing. Specimens that had a low modulus pad composed of sintered FeNiCrAlY fibermetal survived 1000 thermal shock cycles without spalling of the ceramic, representing a thermal shock life about three times that of the previous baseline. A "figure of Merit" for the low modulus pad materials taking into consideration the elastic modulus, thermal conductivity, strength, and oxidation resistance of the pad was proposed, and showed reasonable agreement with the thermal shock results. A potential surface distress problem on the zirconium oxide, associated with non-uniform surface temperature distribution and rapid stress relaxation was identified. One approach to solving the surface distress problem through application of laser surface fusion of the zirconium oxide layer showed some promise,

but improvements in the laser surface fusion process are necessary to prevent process associated damage to the ceramic.

INTRODUCTION

Total fuel consumption by the U. S. airlines is approximately $15/10^9$ gal/yr (ref. 1). With the increasing cost of petroleum derived fuels, there is strong incentive to improve the efficiency of aircraft gas turbine engines. A very effective way of improving gas turbine engine efficiency is to reduce gas path seal clearances throughout the engine. In most cases, the single most significant gas path seal location is over the high pressure turbine blade tip, where from 1% to 3% improvement in turbine efficiency may be realized for each 1% reduction in tip clearance to turbine blade span ratio (ref. 2). Depending on engine type and design, 1% to 3% improvement in turbine efficiency is equivalent to about a 0.5% to 1% reduction in SFC, or a fuel savings of up to 150×10^6 gal/yr in the U. S. commercial airline fleet.

The key to maintaining minimum clearance over the high pressure turbine blade tip is to provide a suitable stationary shroud material. Currently used materials are metallic and are prone to gradual clearance degradation through erosion and corrosion. Also, in the event of rub interactions with the blade tips, they tend to cause blade tip wear, i.e., they are not very abradable.

Ceramic material systems based on the use of plasma-sprayed yttria stabilized zirconium oxide (YSZ) in conjunction with a structural metallic backing provide a promising alternative to the currently used metallic system. The most significant concern in regard to the plasma-sprayed YSZ systems is to provide resistance to cracking and spalling

due to thermal stress and prolonged exposure to high temperatures. Two approaches to reducing thermal stresses in the YSZ seal system are being pursued. One is to grade the properties in either a stepwise or a continuous manner by grading composition from fully metallic adjacent to the metallic backing to fully ceramic adjacent to the gas path. This method is summarized in ref. 3. The other approach incorporates a low density, low modulus metallic pad or cushion between the ceramic layer and the metallic substrate as described by Erickson (ref. 4). The function of the low modulus pad material is to decouple the YSZ layer from the metallic substrate so that thermal distortion mismatches between the substrate and the YSZ layer do not give rise to large thermal stresses. A number of candidate low modulus pad materials were evaluated in cyclic thermal shock testing as reported in ref. 5.

The objectives of this work were to (1) experimentally evaluate candidate composite wall concepts with low modulus strain isolator pad materials, (2) identify a guideline for selection and development of the low modulus materials, and (3) identify further problem areas that need to be addressed. Specimens were evaluated in cyclic thermal shock testing by alternately holding them directly in an oxy-acetyline torch flame, then subjecting them to a cooling air blast. Performance was judged on the basis of the number of cycles required to spall the ceramic material from the substrate, with 1000 cycles selected as run-out. One thousand cycles was considered significant with respect to the total accumulated time at temperature (50 hrs) considering diffusion, creep, and oxidation related mechanisms. Also, 1000 cycles is considered significant with respect to engine service.

APPARATUS AND PROCEDURE

The cyclic thermal shock apparatus is shown in Figure 1. An oxygen-acetylene torch provides the means of heating the specimen when it is in the "heat-up" position, with the flame impinging directly onto the ceramic surface at a 90° angle. While the ceramic surface is being heated, cooling air is directed onto the specimen backing. The flame is positioned and tuned so that during the heat-up phase the ceramic surface reaches a stable temperature of about 1315° C within one minute for all seal configurations. Total duration of the "heat-up" phase is 3½ minutes. Cooling air flow to the backing is controlled to 2.4×10^{-3} m^3/sec (5 ft^3/min) for all specimens, with associated backing temperatures of 480° to 540° C, depending on specimen configuration. Ceramic surface temperatures are monitored by an infra-red pyrometer, and were cross-checked by chromel alumel thermocouples embedded in a few special calibration specimens. Temperatures at other locations in the seal and on the metallic backing are measured by chromel-alumel thermocouples in all specimens.

After being held in the flame for 3½ minutes, the specimen is moved by means of the pneumatic actuator into the "cool-down" position. During the cool-down phase, which lasts for 1 minute, a cooling air flow of 1.2×10^{-3} m^3/sec (2.5 ft^3/min) is directed onto the ceramic surface in addition to the 2.41×10^{-3} m^3/sec (5 ft^3/min) flowing over the back surface. The ceramic surface was thereby cooled from its maximum of 1315° C to about 450° C in several seconds. By the end of the cool-down phase the entire specimen is at about 300° C. The cycle is then

repeated. A representative time-temperature schedule for the entire thermal cycle is shown in Figure 2. Temperatures are indicated for the ceramic surface and the metallic backing.

MATERIALS

The specimens evaluated in this study incorporated a low modulus strain isolator pad between the dense metal substrate and the plasma-sprayed ceramic layer. The function of the low modulus strain isolator pad was to allow the ceramic layer and the metal backing to undergo thermal expansion and contraction independently of one-another. The overall specimen configuration is depicted in Figure 3.

Specimens were prepared by first brazing or plasma-spray depositing the porous metal low modulus pad material onto a dense 2.54 cm x 5.08 cm 304 stainless steel substrate. The substrate was 0.95 cm thick. The braze used was PAL 1, a gold-nickel palladium-braze foil. The low modulus materials evaluated along with compositional and structural information are listed in Table I. The materials are designated LM-1 through LM-7 for convenience, LM-1 being the baseline low modulus material consisting of a 35% dense sintered Hoskins 875 wire (125 μm diameter) structure. LM-1 material is the Brunswick Corporation Brunsbond material. In all cases except LM-5, the low modulus pad was 3.2 mm thick. The LM-5 layer, prepared by plasma-spray deposition, was about 1.6 mm thick.

The next step, after brazing the low modulus pad to the substrate, was to apply a 50 μm NiCrAlY bondcoat directly onto the exposed pad

surface. The NiCrAlY was plasma spray deposited using a Plasmadyne SG-1 gun and the following spray parameters: 350 ampere arc current, 4.2×10^{-4} m^3/sec arc gas (Argon) flow rate, 9.3×10^{-5} m^3/sec powder gas flow rate with the powder feed setting at 23, using the forward plasma feed port. The powder composition was Ni-16 w/o Cr-6w/oAl-0.6w/oY. Powder particle size was in the range -200 + 325 mesh size.

After applying the bondcoat, the yttria stabilized zirconium oxide layer was applied. The powder employed was ZrO_2 - 12w/oY_2O_3, and the particle size was -200 + 325 mesh. Using the Plasmadyne SG-1 plasma spray gun, the following parameters were employed: 550 ampere arc current, 4.6×10^{-4} m^3/sec arc gas (Argon) flow rate, 9.3×10^{-5} m^3/sec powder gas flow rate, with the powder feed setting at 3.0. The plasma-sprayed yttria stabilized zirconium oxide coating, henceforth referred to as YSZ, was deposited to a thickness of about 2.1 mm. The plasma-sprayed materials and parameters are essentially those developed by Liebert and Stecura (ref. 6) for thermal barrier application.

RESULTS AND DISCUSSION

Cyclic thermal shock resistance

The cyclic thermal shock results obtained from specimens incorporating various low modulus pad materials are shown in Figure 4. The moduli of elasticity of the low modulus pad materials are indicated on the abscissa. The best performance was obtained from specimens incorporating the sintered FeNiCrAlY fibermetal pad, that is, the LM-6 system. These specimens consistently survived 1000 thermal shock cycles without spalling, about three times the life of the previous

baseline, LM-1. Metallographic sections made from specimens that had survived 1000 cycles are shown in Figure 5, and reveal some degree of cracking near the interface between the YSZ layer and the NiCrAlY bondcoat. Laminar cracking is most apparent in the areas where normal cracks have propagated through the YSZ layer to the bondcoat. Much of the interface, however, is still intact.

In general, the results summarized in Figure 4 do not show a consistent correlation between thermal shock resistance and modulus of elasticity of the low modulus pad, despite increased strain isolator effectiveness of low modulus materials as the modulus of elasticity decreases. To the left of the demarcation line indicated in Figure 4, early failures occurred within the low modulus pad and were related to oxidation of the fiber to fiber bonds in the pad material, as discussed in ref. 5. The effectiveness of the low modulus pad as a strain isolator did not bear on the failure mechanism. The higher modulus pad materials to the right of the demarcation line were generally stronger and more oxidation resistant than those to the left of the line. Failures, when they occurred, initiated at or near the YSZ/bondcoat interface as illustrated in Figure 6.

The above observations suggest that a factor incorporating the strength, thermal conductivity, elastic modulus and some measure of oxidation resistance of the low modulus pad material might provide better correlation with thermal shock resistance of the seal systems tested than would elastic modulus alone. The factor, if it is to be used as a "figure of merit," should increase as the elastic modulus

of the pad material decreases because of an overall reduction in thermal stresses throughout the seal with decreasing pad modulus. From the standpoint of durability of the low modulus pad itself, the proposed factor should increase with increasing strength and oxidation resistance of the pad material. Also, the factor should increase as the thermal conductivity of the pad increases since temperatures in the pad decrease (ref. 7) with increasing conductivity, and hence pad durability would be expected to increase. A suggested factor incorporating all of the above mentioned considerations is:

$$G = \frac{K\sigma T_{ox}}{E}$$

where K is the thermal conductivity, σ the tensile strength and E the elastic modulus of the low modulus pad material. T_{ox} is an oxidation threshold temperature defined as the temperature at which the depth of oxidation equals the average particle-to-particle bond dimension characteristic of the pad material in a prescribed time. Obviously, for a given alloy composition and particle size and morphology for the pad material, the properties included in the suggested factor cannot be varied independently. However, the factor G does provide a means of correlating the thermal shock resistance of seal systems incorporating various different types of low modulus pad materials.

As may be seen in Figure 7, the cyclic thermal shock lives of the various systems evaluated do in fact generally increase with increasing G, a simple linear correlation shown for illustrative purposes. For purposes of this correlation, T_{ox} used in G was defined as the temperature at which under static oxidation conditions oxide film growth would

be expected to penetrate to a depth equivalent to the average particle size for the low modulus pad material. The material properties used to calculate the appropriate value of G for each low modulus pad material are summarized in Table II.

The significance of the suggested figure of merit G would probably be increased if accurate property data at operating material temperatures were used. Also, more thorough analyses might suggest something other than the rather simple proportionalities to the proposed material properties. Nevertheless, the idea of using a factor like G as a figure of merit in selecting or developing low modulus pad materials appears to be justified.

Observations of ceramic surface distress

With successful evaluation of low modulus pad supported plasma-sprayed YSZ ceramic turbine seal systems to 1000 thermal shock cycles, and the proposal of a reasonably consistent low modulus pad figure of merit, it would appear that the thermal shock resistance problem is well in hand. Though spalling of the ceramic layer can be controlled, some distress to the ceramic surface is in evidence after 600 cycles. The distress, shown in Figure 8, is in the form of localized pitting about 125 μm (5 mils) deep. The pitting was confined to the "hot spot" regions on the ceramic surface resulting from imperfect temperature distribution during thermal shock cycling. The color pyrometry pattern of specimens in the high temperature steady state portion of the test cycle indicate temperature variations of 200 to 300° C over the ceramic surface, the hottest region in the specimen center.

The mechanism believed to promote the observed surface pitting is illustrated schematically in Figure 9. The key considerations are: (1) local hot regions 1 to 2 cm wide near the center of the specimen are initially subjected to high compressive stresses on the order of 15 to 20 MN/M^2; (2) the compressive creep rate of plasma-sprayed YSZ, being on the order of several percent per hour under conditions prevailing near the ceramic surface, leads to rapid stress relaxation; (3) after considerable relaxation of the high temperature compressive stresses near the surface has occurred, high tensile stresses prevail in those regions upon cool-down; (4) tensile stresses lead to crack initiation in the ceramic surface resulting in a very fine mudflat crack pattern. The cracks propagate to a depth comparable to the depth to which stress relaxation had occurred. With continued cycling the mudflat cracks propagate as laminar cracks due to gradual shrinkage of material on the ceramic surface. The growth of laminar cracks partially decouples the mudflat cracked surface from the substrate, causing material to "peel-up" as shown in Figure 9, leading to very high local temperatures around the crack edges and accelerated surface deterioration. A metallographic section through such a distressed surface region (Fig. 10), reveals the progression of shallow pit formation described.

One way of addressing the surface pitting problem is to provide a surface layer on the plasma-sprayed ceramic that is resistant to high rate stress relaxation under seal operating conditions. Experiments have been conducted on specimens which had been subjected to a laser fusion surface treatment prior to test. Laser fusion of the surface

resulted in a 125 μm deep, nearly fully dense layer of YSZ integrally bonded to the plasma sprayed YSZ substructure, as shown in Figure 11. Laser fusion of the surface was effected by scanning the plasma-sprayed YSZ surface of a specimen with a 175 watt continuous wave CO_2 laser.

The results obtained so far from specimens incorporating the laser fused surface treatment are not too conclusive. As may be seen in Figure 11, cracks are present in the fused layer, and macroscopic examination of the fused surface revealed the presence of a very fine crack network enclosing cells about 1 mm in diameter. It is believed that these particular cracks are beneficial from a stress relief and crack growth retardation standpoint. In fact, one seal specimen incorporating the LM-1 low modulus pad and laser fusion treatment to the YSZ surface survived 1000 thermal shock cycles without spalling and without any observable laminar cracking in the area of the YSZ/bondcoat interface. As for surface pitting, the results are difficult to assess. No pitting or other surface distress was evident after 300 test cycles. However, looking again at Figure 11, laminar cracks may also be seen (pre-test condition) about 75 μm below the fused surface layer. After 500 test cycles, some of these cracks had apparently propagated, joining some of the longer normal cracks, and platelets of ceramic material about 250 μm thick began to spall from the surface. This was followed by a gradual deterioration of the plasma sprayed YSZ layer, so that after 1000 cycles the specimen appeared as shown in Figure 12.

Subsequent tests on specimens with the laser fused surface are consistent with the results described above. There does appear to be

tentative evidence that the onset of stress relaxation related surface distress is at least delayed, if not eliminated. Before full assessment of this technique is possible, the process will have to be adjusted to minimize the subsurface laminar crack damage initiate by the laser fusion process.

CONCLUSIONS

Based on the results of this study, the following conclusions are reached:

1. The best low modulus pad material evaluated consisted of sintered 35% FeNiCrAlY fibermetal. Specimens incorporating this pad material consistently survived 1000 thermal shock cycles, about 3x the number survived by the previous best system. Further improvements in the YSZ/bondcoat interface region are needed.

2. A first cut "figure of Merit" for low modulus pad materials, combining the effects of material strength, modulus, thermal conductivity and oxidation resistance in the form of $G = \frac{K\sigma T_{ox}}{E}$ is shown to be consistent with cyclic thermal shock resistance. In general, the higher the number G, the more effective is the low modulus pad material.

3. A potential problem associated with local stress relaxation near the YSZ surface due to non-uniform temperature distribution was identified. Laser fusion of a thin surface layer of YSZ showed some promise as a means of reducing this particular problem, but the laser fusion surface treatment itself needs improvement in order to eliminate wear surface laminar cracks.

REFERENCES

1. Dugan, J. F., et al., "Fuel-Conservative Engine Technology," Aeronautical Propulsion, NASA SP-381, 1975, pp. 157-190.

2. Roelke, R. J., "Miscellaneous Losses - Tip Clearance and Disk Function," Turbine Design and Applications, Vol. 2, A. J. Glassman, ed., NASA SP-290, 1973, pp. 125-148.

3. Bill, R. C., Shiembob, L. T., Stewart, O. L., "Development of Sprayed Ceramic Seal System for Turbine Gas Path Sealing," NASA TM-79022, 1978.

4. Ericson, A. F., Nablo, J. C., and Panzera, C., "Bonding Ceramic Materials to Metallic Substrates for High-Temperature Low-Weight Applications," ASME Paper No. 78-WA/GT-16, Dec. 1978.

5. Bill, R. C., Wisander, D. W., Brewe, D. E., "Preliminary Study of Methods of Providing Thermal Shock Resistance to Plasma Sprayed Ceramic Gas Path Seals," NASA TP-1561, 1980.

6. Stecura, S., and Liebert, C. H., "Thermal Barrier Coating System," U. S. Patent No. 4,055,705, Oct. 1977.

7. Kennedy, F. E., and Bill, R. C., "Thermal Stress Analysis of Ceramic Gas-Path Seal Components for Aircraft Turbines," NASA TP-1437, 1979.

TABLE I. - COMPOSITION AND STRUCTURE OF LOW MODULUS PAD MATERIALS

Designation	Alloy composition (wt %)	Particle diameter (μm)	Density (%)	Hardness (R_{15Y})
LM-1	Hoskins 875	125	35	25 R_{15Y}
LM-2	Hastelloy-X	10	21	85 R_5 (-180 R_{15Y})
LM-3	Fe-20Cr-6Al-.02Y	17	21	82 R_{5Z} (-190 R_{15Y})
LM-4	Ni-15Cr-5Al	50	40	52 R_{15Y}
LM-5	Ni-16Cr-6Al-.6Y	80	50	49 R_{15Y}
LM-6	Fe-25Ni-18Cr-9Al -.02Y	35	32	49 R_{15Y}
LM-7	Fe-25Ni-18Cr-9Al -.02Y	17	21	83 R_{5Z} (-90 R_{15Y})

TABLE II. - PROPERTY VALUES FOR LOW MODULUS PAD MATERIALS

Designation	Thermal conductivity, W/m ^{o}K	Tensile strength, MN/m^2	Elastic modulus GPa	Temperature limit, ^{o}K	G W/m
LM-1	1.25	30	6.3	1423	7.9
LM-2	.35	10	1.7	991	2.0
LM-3	.35	10	1.2	1227	3.6
LM-4	.25	13	3.5	1255	3.3
LM-5	1.5	15	10	1255	2.8
LM-6	1.6	20	5.9	1325	7.1
LM-7	.35	10	1.7	1227	2.6

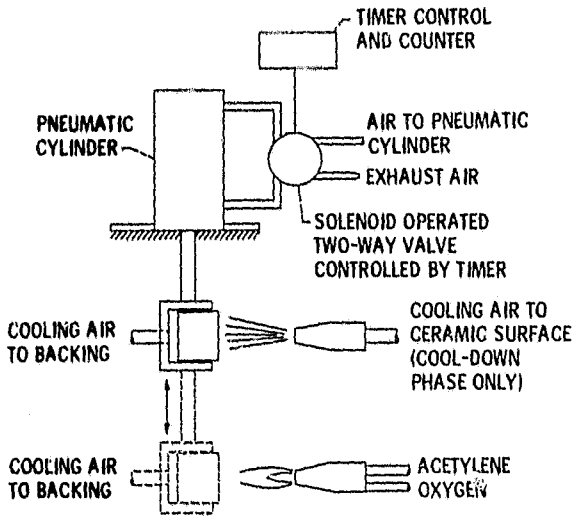

Figure 1. - Cyclic thermal shock apparatus.

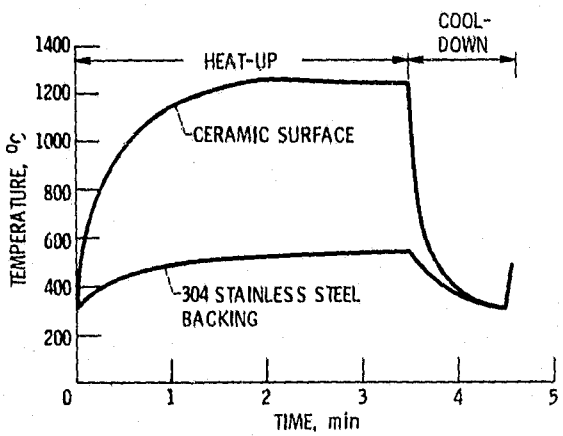

Figure 2. - Representative time-temperature plot for thermal shock cycle.

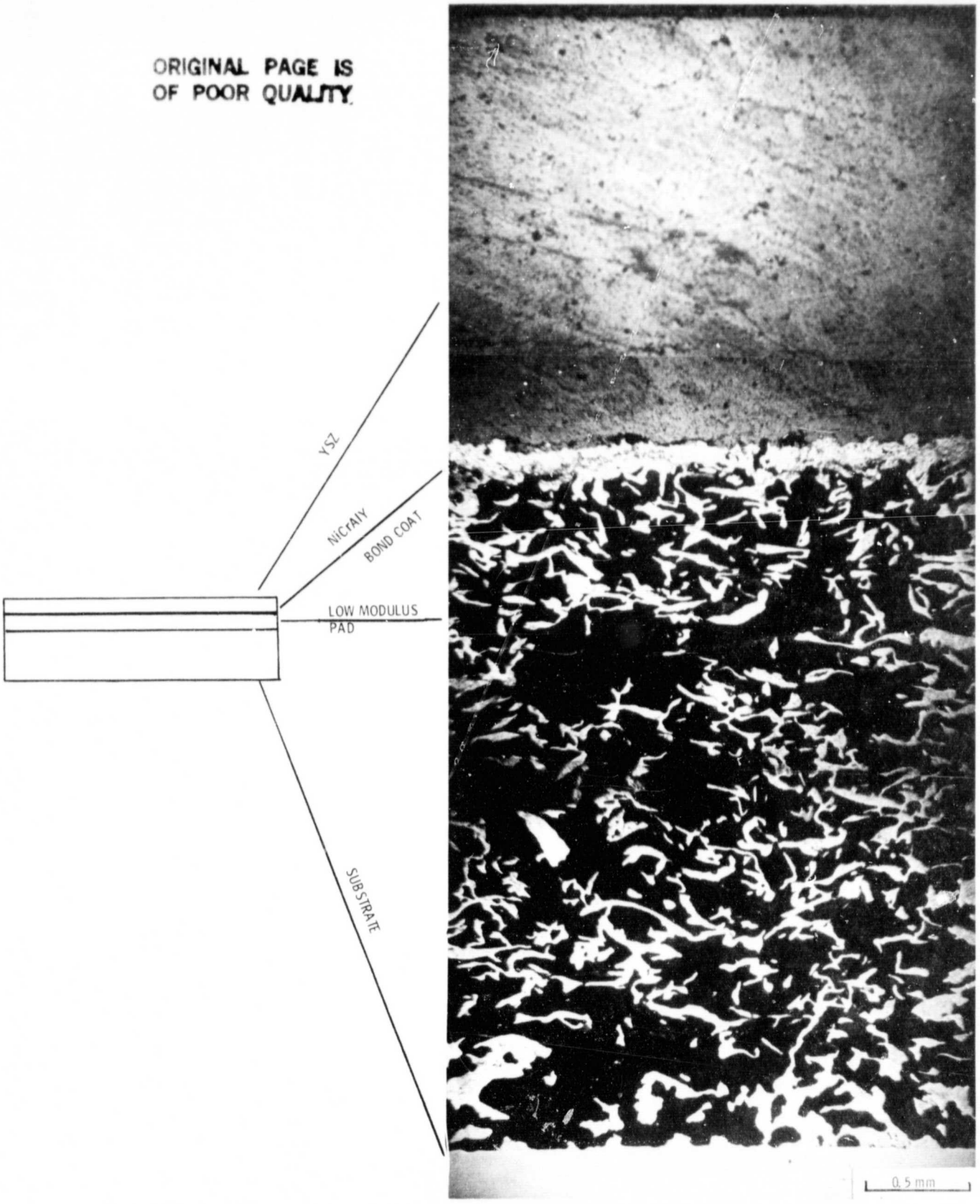

Figure 3. - Thermal shock test specimen configuration.

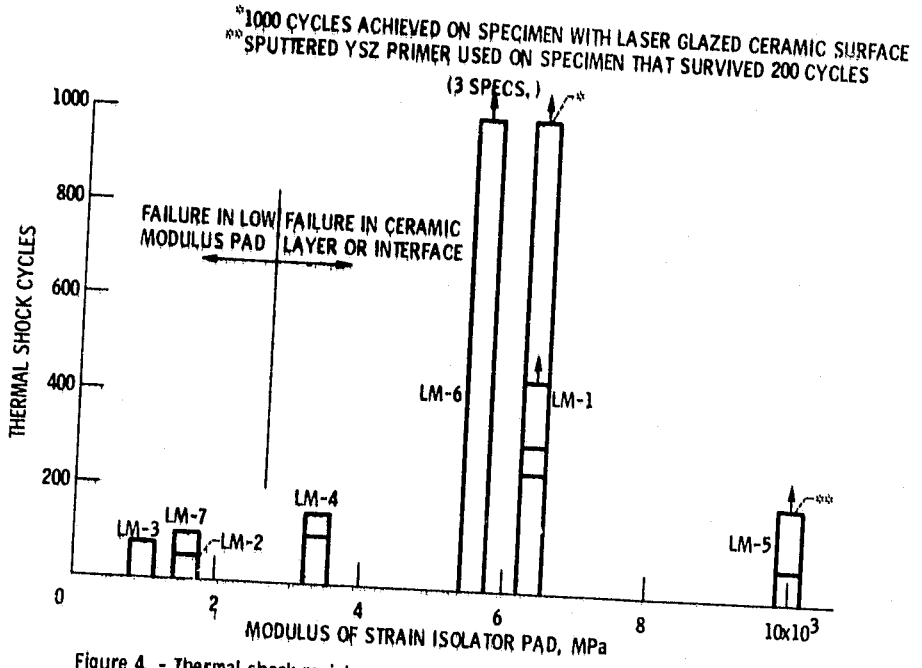

Figure 4. - Thermal shock resistance versus modulus of elasticity of strain isolator pad.

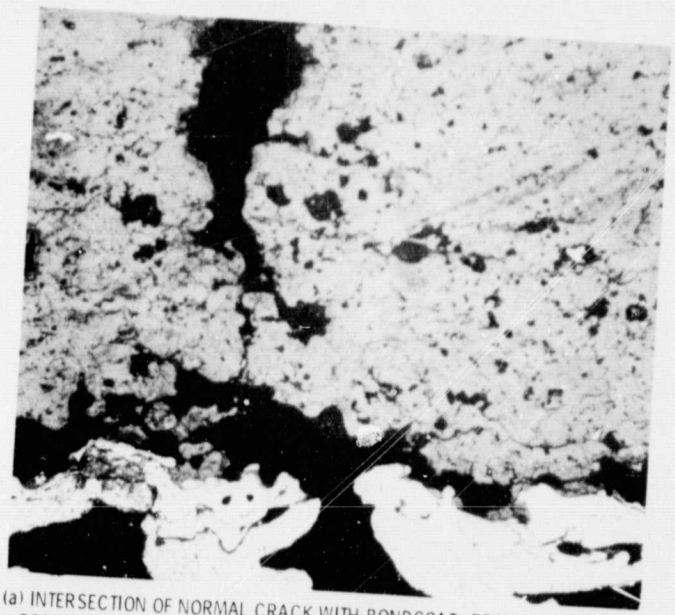

(a) INTERSECTION OF NORMAL CRACK WITH BONDCOAT, RESULTING IN BOND-COAT FISSURE AND LAMINAR CRACKS.

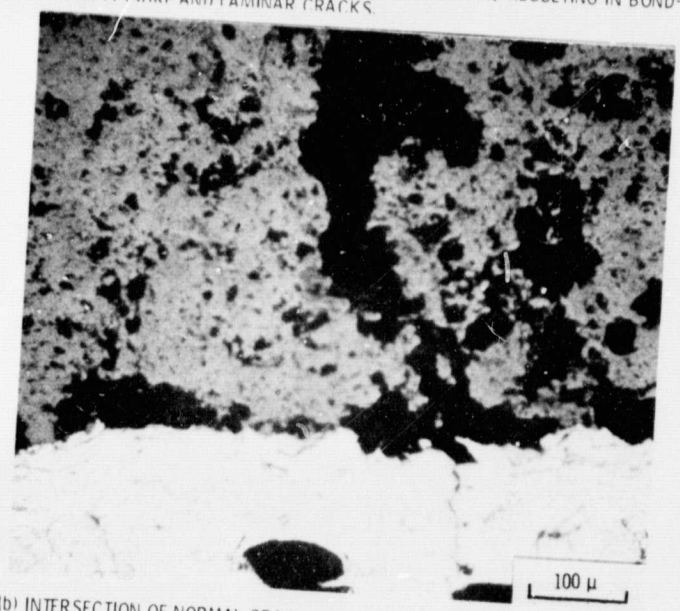

(b) INTERSECTION OF NORMAL CRACK WITH BONDCOAT, RESULTING IN BOND-COAT CRACK AND LAMINAR CRACKS.

Figure 5. - Metallographic sections through LM-6 specimen after 1000 thermal shock cycles showing condition of the YSZ/bondcoat interface region. Material in the upper portion of each photograph is YSZ. The lighter material in the lower portion is the NiCrAlY bondcoat.

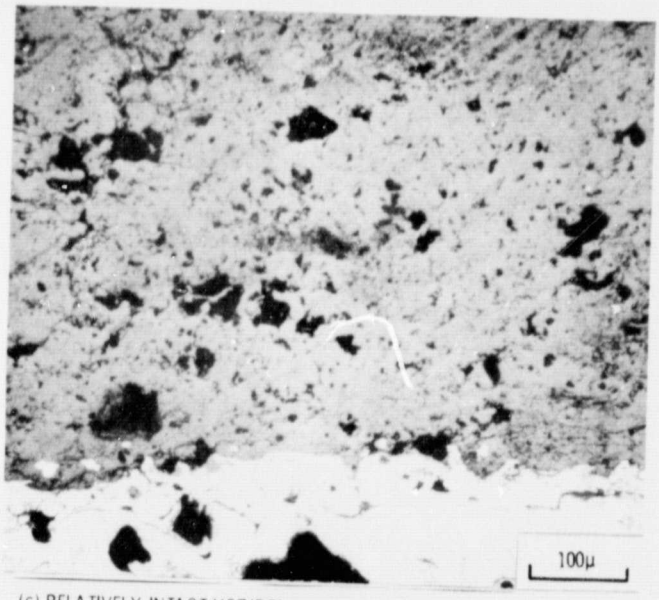

(c) RELATIVELY INTACT YSZ/BONDCOAT INTERFACE, REMOTE FROM ANY NORMAL CRACKS.

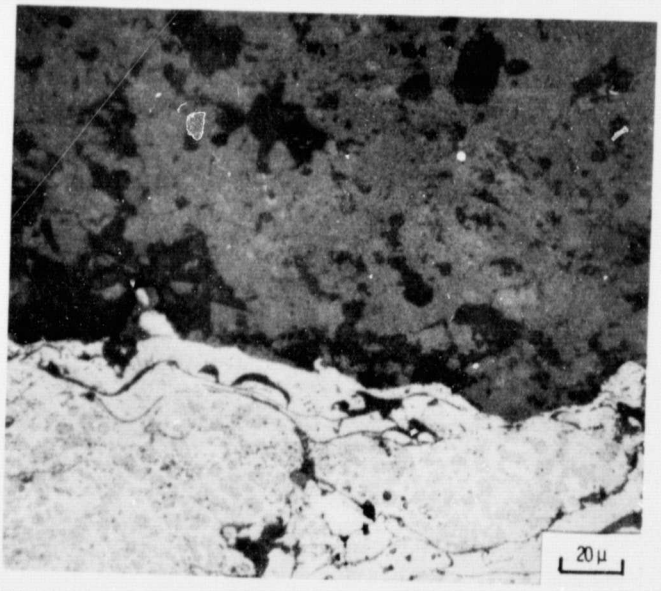

(d) YSZ/BONDCOAT INTERFACE SHOWING ISOLATED LAMINAR CRACKING.

Figure 5. - Concluded.

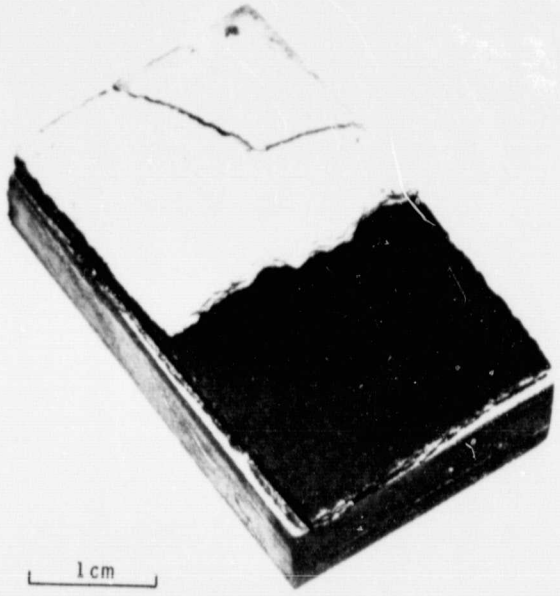

C-79-664

Figure 6. - Example of failure that had occurred near the YSZ/bondcoat interface.

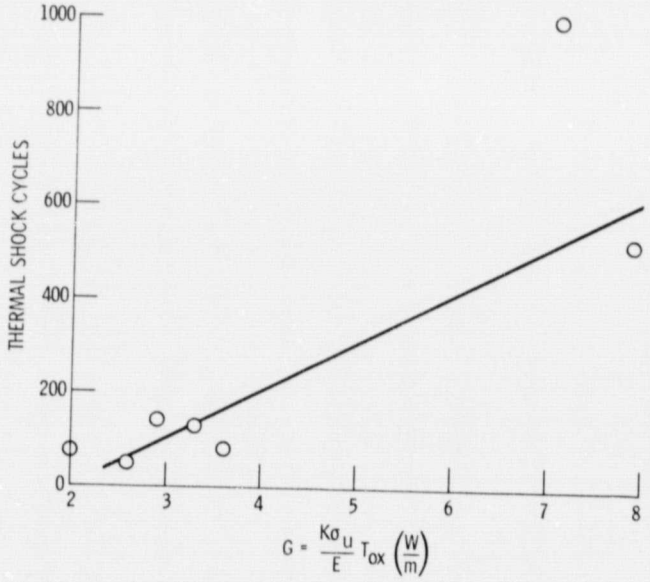

Figure 7. - Thermal shock resistance versus the parameter G.

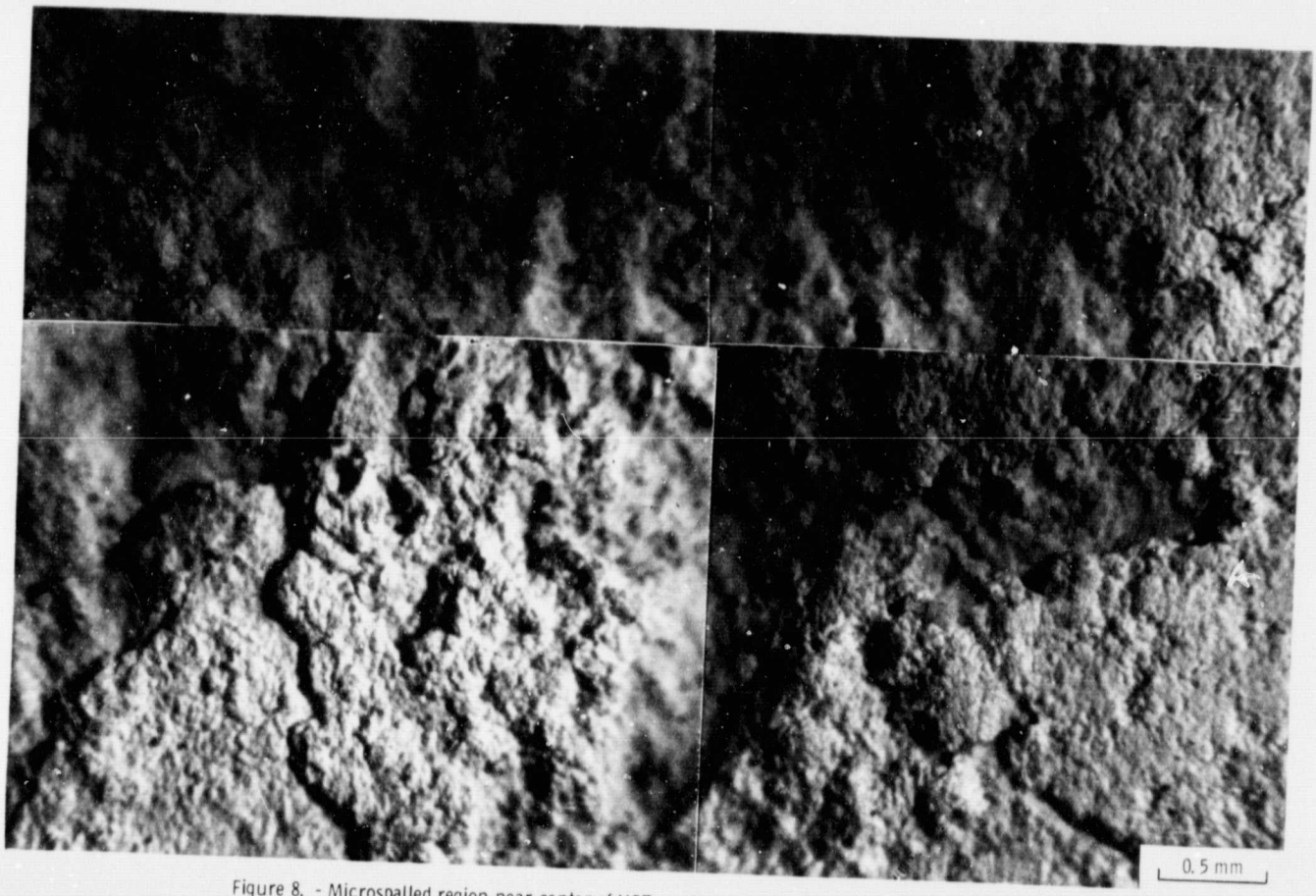

Figure 8. - Microspalled region near center of YSZ surface, as seen after 600 thermal shock cycles.

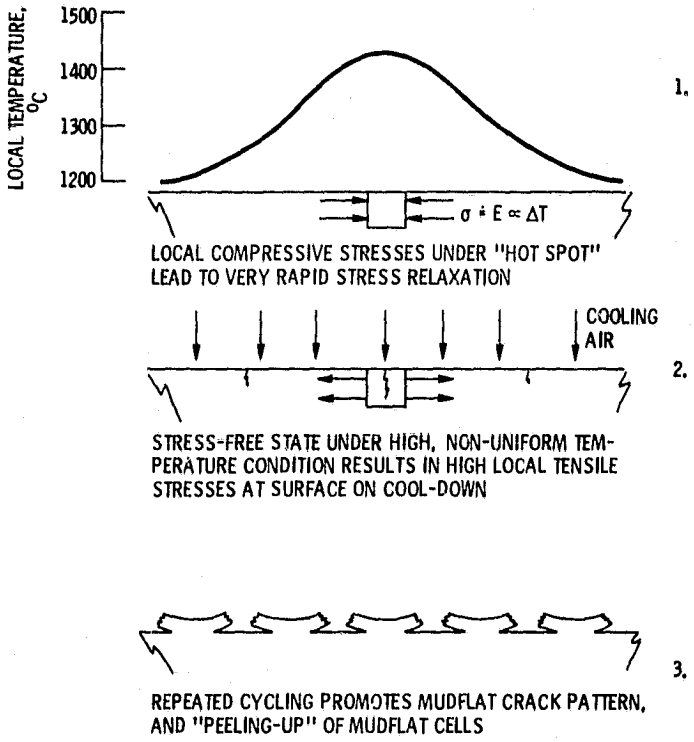

Figure 9. - Steps in the progressive deterioration of plasma-sprayed YSZ surface under conditions of intense non-uniform temperature distribution.

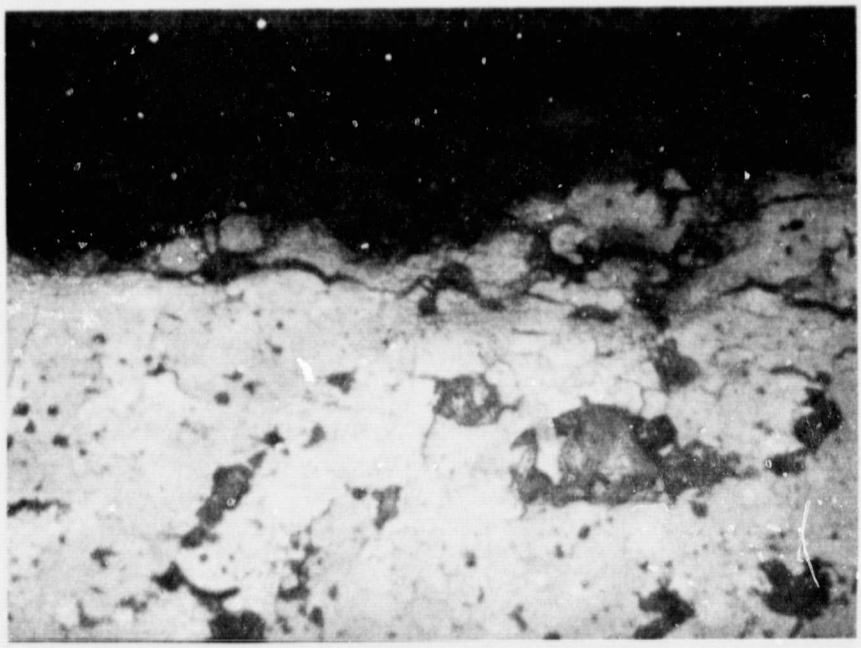

(a) CENTER OF LM-6 SPECIMEN AFTER 1000 THERMAL SHOCK CYCLES.

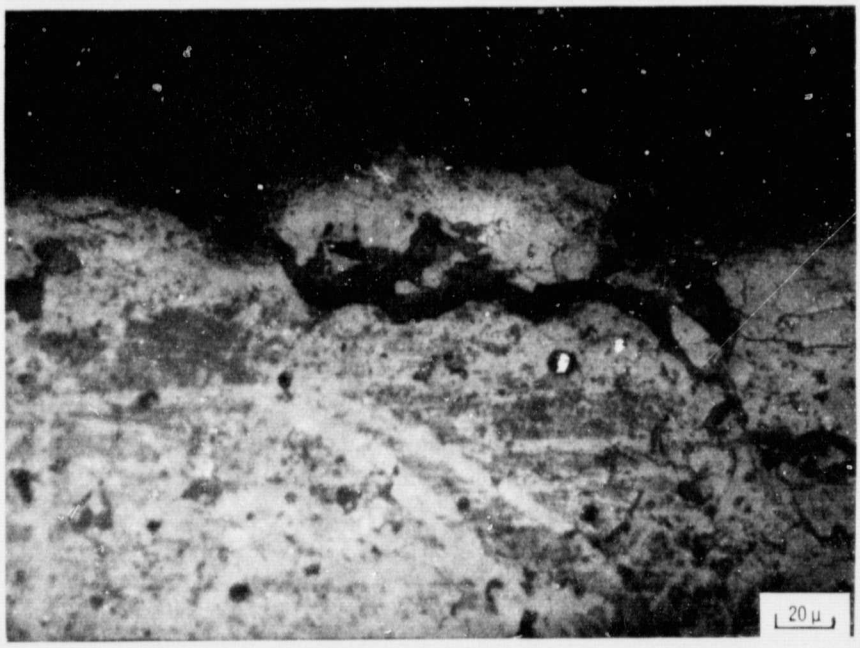

(b) 1 cm FROM END OF LM-6 SPECIMEN AFTER 951 THERMAL SHOCK CYCLES.

Figure 10. - Sections through the YSZ surface of two LM-6 specimens revealing details of the micropit mechanism of surface deterioration. The very fine material in the cracks and on the surface itself appeared as white "flour like" debris on the specimen.

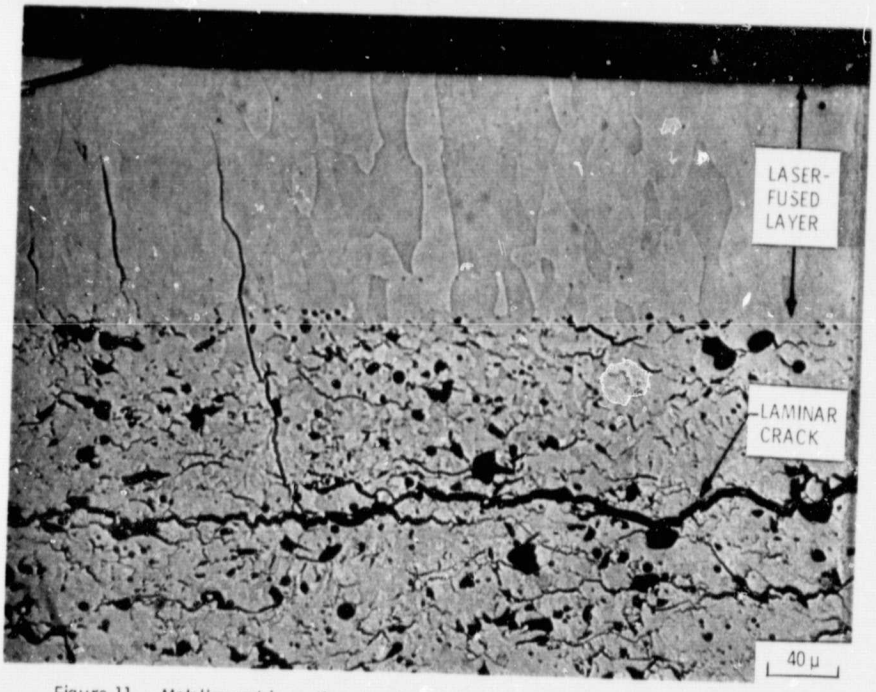

Figure 11. - Metallographic section showing laser fused surface layer on YSZ (pretest).

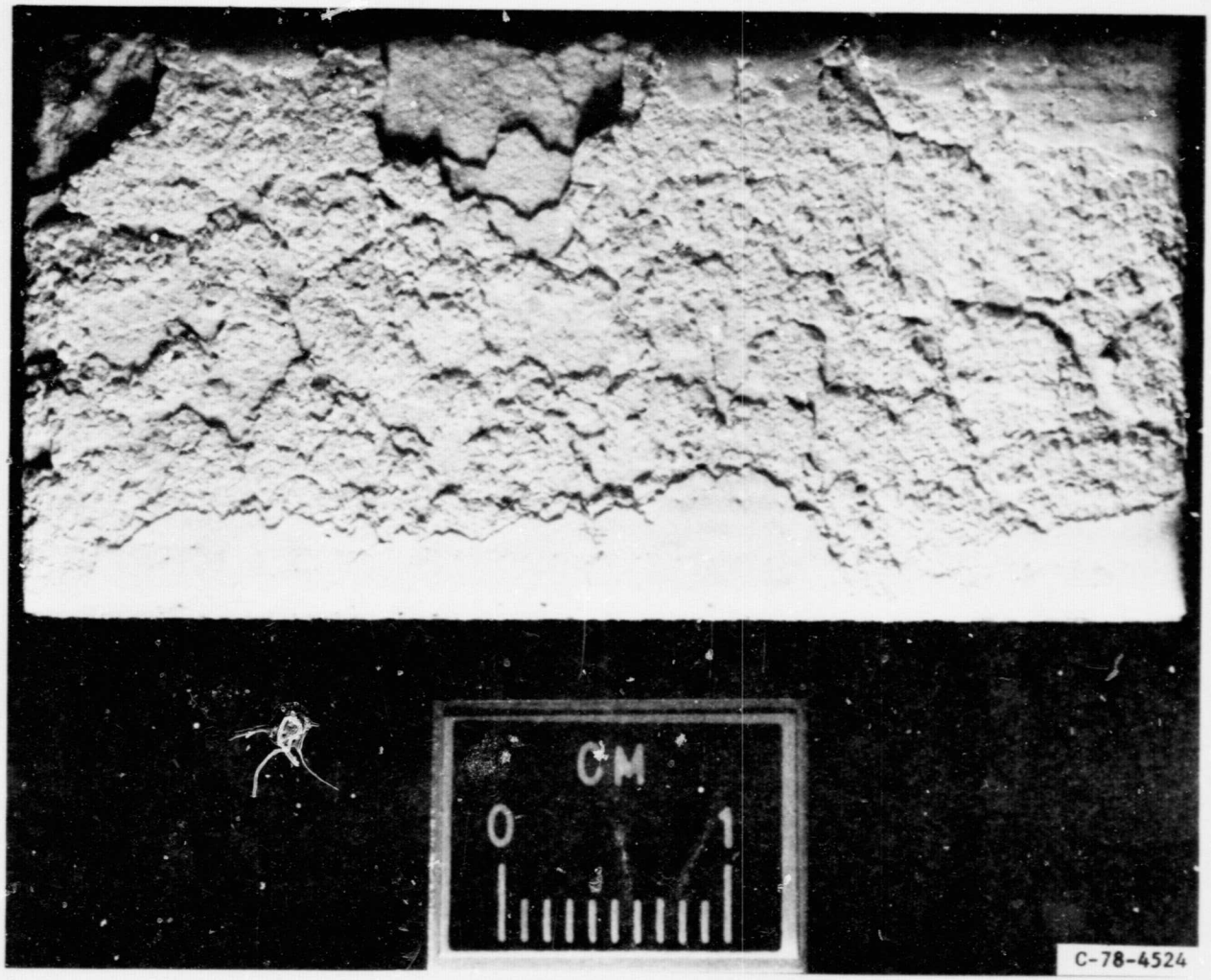

Figure 12. - Ceramic turbine seal with laser fused surface and LM-1 strain isolator pad after 1000 thermal shock cycles.